

GAN-based Massive MIMO Channel Model Trained on Measured Data

Florian Euchner, Janina Sanzi, Marcus Henninger, Stephan ten Brink
Institute of Telecommunications, Pfaffenwaldring 47, University of Stuttgart, 70569 Stuttgart, Germany
{euchner,henninger,tenbrink}@inue.uni-stuttgart.de

Abstract—Wireless channel models are a commonly used tool for the development of wireless telecommunication systems and standards. The currently prevailing geometry-based stochastic channel models (GSCMs) were manually specified for certain environments in a manual process requiring extensive domain knowledge, on the basis of channel measurement campaigns. By taking into account the stochastic distribution of certain channel properties like Rician k -factor, path loss or delay spread, they model the distribution of channel realizations. Instead of this manual process, a generative machine learning model like a generative adversarial network (GAN) may be used to automatically learn the distribution of channel statistics. Subsequently, the GAN’s generator may be viewed as a channel model that can replace conventional stochastic or raytracer-based models. We propose a GAN architecture for a massive MIMO channel model, and train it on measurement data produced by a distributed massive MIMO channel sounder.

Index Terms—channel model, generative adversarial network, massive MIMO

I. INTRODUCTION

Channel modeling is essential in communications engineering. Fundamental theoretic results are often derived starting from some of the simplest channel models (e.g., memoryless discrete-time and discrete-value channels or additive white Gaussian noise (AWGN) channels) and proposals for practical waveforms and modulation formats are motivated using simple stochastic channel models (e.g., Rician Fading, or Clarke’s model [1]). More involved channel models have been developed for researching practical wireless communication systems, that must be able to withstand various degrees of frequency- and/or time-selective fading, hardware impairments and other effects. One such channel model was proposed by the 3rd Generation Partnership Project (3GPP) for the frequency range 0.5 – 100 GHz in technical report (TR) 38.901 [2], which is an example for a so-called geometry-based stochastic channel model (GSCM). These channel models define a set of stochastic parameters, including information about the distribution of delay spreads or path loss exponents, and guarantee some level of spatial coherence, for example by ensuring the spatial distribution follows some three-dimensional, correlated noise process. While stochastic channel models usually only define the model (e.g., procedures, distributions, parameters), channel simulators like Quasi Deterministic Radio Channel Generator (QuaDRiGa) [3] may

This work is supported by the German Federal Ministry of Education and Research (BMBF) within the projects Open6GHub (grant no. 16KISK019) and KOMSENS-6G (grant no. 16KISK113).

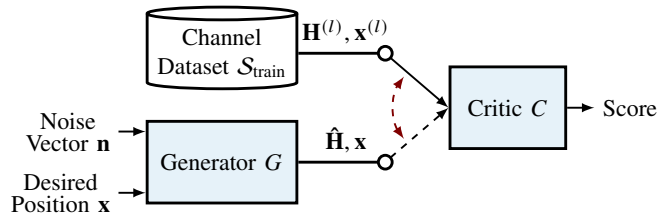


Fig. 1. Structural overview of the Wasserstein GAN for channel modeling. The generator G learns the CSI distribution of the channel.

be used to produce channel realizations, for example in the form of channel impulse responses (CIRs). For even better spatial consistency, raytracing-based channel simulators may be used as channel models [4]. As evidenced by lots of successful, recent research based on stochastic or raytracer-based channel models, these existing solutions work well for the intended purposes. However, in both cases, there is a lot of manual work required to come up with a model: To obtain a stochastic channel model that describes a certain environment for a set of system parameters (e.g., carrier frequency), one first has to obtain channel measurements for the particular environment, to then identify relevant stochastic parameters and to finally extract these parameters from the measurements. The inherent danger in this process is that relevant parameters may be overlooked or that the modeled environment simply does not match the system the model is used for. Aforementioned TR 38.901 channel model is only valid for a limited set of manually selected scenarios of interest, which define environments labeled, for example, “urban macrocell” or “indoor factory”.

Raytracing-based channel models offer more flexibility to the user, but require significantly more effort related to the definition of the 3D model and material properties. What is more, the user of a channel model may not care about specifics of one particular environment, which a raytracing-based channel model offers, but may want to rather evaluate some system on a certain type of environment. While raytracing may be used to model an environment in a faithful, consistent way, stochastic channel models provide more variety and randomness in their channel realizations. Finding a trade-off between faithfulness and randomness is a rather fundamental issue in channel modeling, and the right balance has to be determined depending on the particular application.

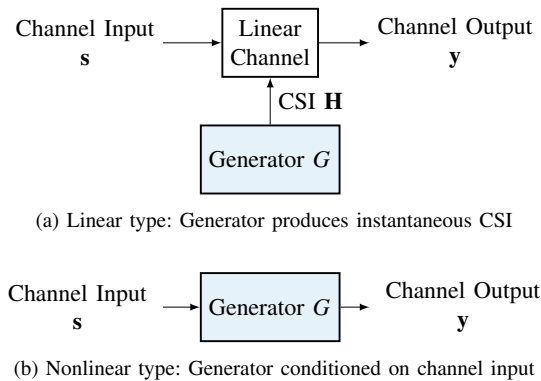


Fig. 2. Different types of GAN-based channel models.

This work¹ analyzes a generative machine learning-based approach, which can automate the procedure of parametrizing a channel model on measurement data. Instead of specifying relevant stochastic parameters manually, the generative channel model should automatically learn the distribution of the measured CSI, based on samples from one or multiple datasets. In particular, we explore the use of a GAN [5] (a Wasserstein GAN (WGAN) [6] with gradient penalty (GP) [7], to be precise) for automated learning of stochastic channel models. The basic structure of such a GAN-based channel model is illustrated in Fig. 1.

A. Related Work and Contributions

The idea of a GAN-based channel model that learns the CSI distribution, first proposed in [8], has gained some attention in the community [9]–[13]. In [8], the concept of GAN-based channel modeling is introduced on a high level, motivating the idea by showing that a GAN can learn the noise distribution of an AWGN channel. In [9]–[11], a GAN is trained on channel realizations (impulse responses). As an alternative to GANs, [12] investigates the use of diffusion models for channel modeling and [13] compares a GAN-based channel model to a variational autoencoder (VAE)-based model and a diffusion model. In all previous research that the authors are familiar with, the generative model is trained on data that was itself produced by another channel model, usually related to aforementioned 3GPP TR 38.901 GSCM.

In a separate line of work, initiated by [14], various authors have investigated using a conditional GAN to learn the input-output relationship of the channel itself, which is a different type of GAN-based channel model. The distinction between [8] and [14], which is also illustrated in Fig. 2, is the following: In [8], the GAN’s generator produces channel realizations described by CSI in some representation (e.g., time-domain or frequency-domain), as in Fig. 2a. On the other hand, in [14], the generator *becomes* the channel itself: The generator is conditioned on the transmitted signal, and it must attempt to produce a realistic received signal, as in Fig. 2b, which

can be useful e.g. for end-to-end training [15]. We restrict ourselves to the first, linear type of GAN-based channel model as described in [8]. As already outlined in [10], the advantages of generating CSI as an intermediary product are the improved interpretability of the GAN’s output and the better generalization to arbitrary input signals. Furthermore, it ensures that the learned channel is indeed a linear time-invariant (LTI) system, whereas the approach in [14] can learn nonlinear channel models, which is undesirable for modeling physical propagation effects.

The architecture of our neural network draws inspiration from [9], being based on a WGAN with GP. In contrast to all this previous work, however, we train our GAN-based channel model on real-world data measured with a massive multiple-input multiple-output (MIMO) channel sounder, as opposed to the previous efforts which were trained on another channel model. In addition, we investigate the use of a conditional GANs to generate channel realizations at defined locations, while ensuring some level of spatial consistency.

B. Purpose of a GAN-based channel model

The objective of a channel model depends on the application: A GSCM may generate CSI that follows a certain distribution, a raytracer may be used to predict realistic CSI. The purpose of GAN-based channel models has not been well-defined in existing literature. Therefore, we consider two different applications: Using GAN-based channel models as an alternative to GSCMs as a kind of *random generator* for CSI samples, or using GAN-based channel models as a *spatial inter- and extrapolator*, that should ideally predict measured CSI at new locations. While the use of a GAN as an inter-/extrapolator has been suggested to us many times in conversations, we would like to remark that a different neural network structure, like an autoencoder, may be better-suited in that case. In the following sections, we will analyze both types of applications and conclude that, in their current form, GAN-based channel models of linear type are not particularly well-suited for either.

II. SYSTEM MODEL AND MEASUREMENT DATASET

Our objective is to model the distribution of a channel measurement dataset containing L entries, that we refer to as *datapoints* $l = 1, \dots, L$. We model the propagation channel between a distributed massive MIMO antenna system, consisting of B uniform planar arrays (UPAs) with half-wavelength spacing, M_r rows and M_c columns of antennas each, and a single-antenna user equipment (UE). The channel is described by its complex-valued, time-domain CIR. The time-domain CSI tensors can thus be written as $\mathbf{H}^{(l)} \in \mathbb{C}^{B \times M_r \times M_c \times N_{\text{tap}}}$, where N_{tap} is the number of tapped delay line (TDL) taps. Furthermore, we assume that a UE position $\mathbf{x}^{(l)} \in \mathbb{R}^2$ is known for every CSI measurement. Hence, one datapoint is a tuple consisting of CSI tensor and UE position, and the whole dataset may be written as the set

$$\mathcal{S}_{\text{meas}} = \left\{ \left(\mathbf{H}^{(l)}, \mathbf{x}^{(l)} \right) \right\}_{l=1, \dots, L}.$$

¹Partial source code is publicly available at: <https://github.com/Jeijja/GAN-Wireless-Channel-Model>

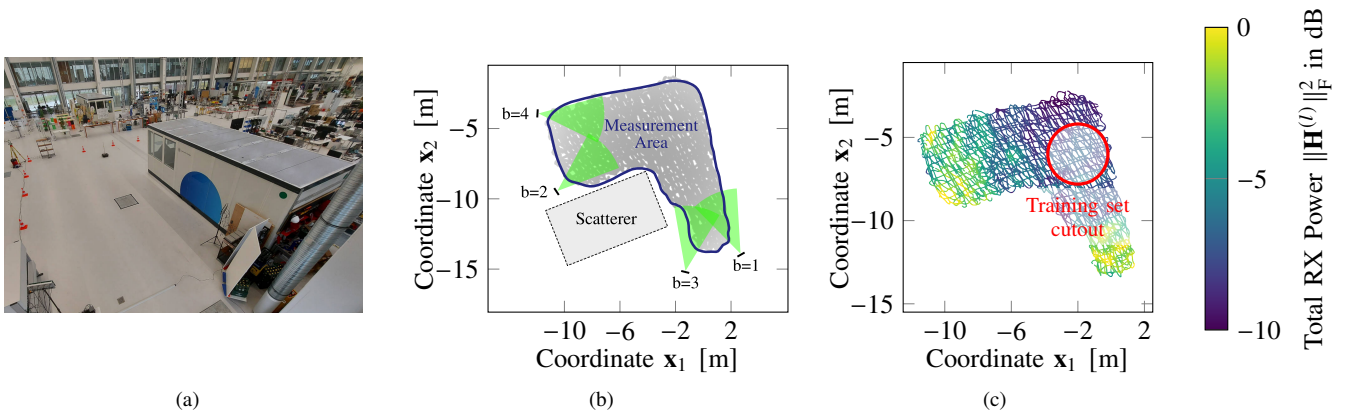


Fig. 3. Information about the environment the dataset was measured in: The figure shows (a) a photograph of the environment, (b) a top view map and (c) a scatter plot with datapoint positions $\mathbf{x}^{(l)}$ in $\mathcal{S}_{\text{meas}}$, colored with the total received power $\|\mathbf{H}^{(l)}\|_F^2$. The antenna arrays in the map are drawn to scale as black rectangles and their directivity is indicated by the green sectors. The received power is normalized such that the maximum received power is 0 dB.

For this work, the dataset $\mathcal{S}_{\text{meas}}$ was measured by *Distributed Channel Sounder by University of Stuttgart (DICHASUS)*, our distributed massive multiple-input multiple-output (mMIMO) channel sounder, whose architecture is thoroughly described in [16]. In brief, DICHASUS is a massive MIMO-orthogonal frequency division multiplex (OFDM) channel sounder. It achieves long-term phase-coherence, even if antennas are distributed. DICHASUS provides large datasets containing OFDM channel coefficients for all antennas and all subcarriers, along with side information like timestamps and accurate information about the positions of all antennas at all times. While measurements are performed in frequency domain, it is only a matter of computing the Fourier transform to obtain the time-domain representation $\mathbf{H}^{(l)}$.

The considered dataset $\mathcal{S}_{\text{meas}}$, containing $L = 83893$ datapoints, is a subset of *dichasus-cf0x* [17], and was captured in an industrial environment with $B = 4$ separate antenna arrays made up of $M = 2 \times 4 = 8$ antennas each. A total of $N_{\text{sub}} = 1024$ OFDM channel coefficients were measured at a carrier frequency of 1.272 GHz and with a channel bandwidth of 50 MHz, though we restrict ourselves to $N_{\text{tap}} = 48$ time-domain taps for all subsequent analyses. The single dipole transmit antenna is mounted on top of a robot, which travels along a set of trajectories inside a defined, L-shaped area, with an overall size of approximately $14 \text{ m} \times 14 \text{ m}$. A photo and a top view map of the environment are shown in Fig. 3. A large metal container is located at the inner corner of the L-shape, blocking the line-of-sight (LoS). The datapoint positions $\mathbf{x}^{(l)}$ are shown in Fig. 3.

We define training set $\mathcal{S}_{\text{train}} \subset \mathcal{S}_{\text{meas}}$ and test set $\mathcal{S}_{\text{test}} \subset \mathcal{S}_{\text{meas}}$ as two disjoint subsets of the complete measurement dataset $\mathcal{S}_{\text{meas}}$. The training set contains $|\mathcal{S}_{\text{train}}| = 17857$ datapoints, the test set contains $|\mathcal{S}_{\text{test}}| = 20973$ datapoints. The training set is used to train the GAN or to parametrize the baselines. The GAN (or a baseline) then generates CSI at the test set locations, and the generated CSI is compared to the true, measured CSI. The test set is obtained from $\mathcal{S}_{\text{meas}}$ by choosing every fourth datapoint. We do the same for the training set, except with an offset, and then additionally cut a

“hole” with a diameter of 4 m into the training set (as visible in Fig. 3c and Fig. 6a). This hole is meant to test the ability of the GAN and baselines to interpolate CSI at previously unseen locations.

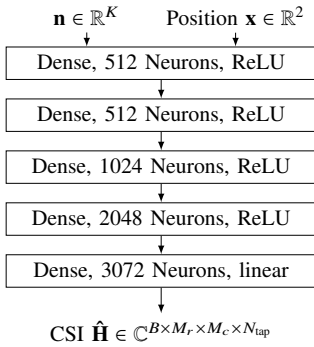
III. GAN-BASED CHANNEL MODEL

Fig. 1 shows the well-known conditional WGAN training setup: For the desired position \mathbf{x} (the condition) and as a function of some noise vector $\mathbf{n} = (n_1, \dots, n_K)$, $n_k \sim \mathcal{N}(0, 1)$, $K = 128$, the generator $G(\mathbf{x}, \mathbf{n})$ produces a *generated* channel realization $\hat{\mathbf{H}} \in \mathbb{C}^{B \times M_r \times M_c \times N_{\text{tap}}}$. As its input, the critic C either receives a *real* (i.e., measured) channel $\mathbf{H}^{(l)}$ from $\mathcal{S}_{\text{train}}$, or a generated channel $\hat{\mathbf{H}}$, always in conjunction with the condition. The critic’s objective is to detect whether the input it receives is real or fake, by assigning a score reflective of the *realness* of the input sample. We train the generator and critic to operate on the *complete* CSI tensors $\mathbf{H}^{(l)}$, which contain time-domain tap coefficients for all $B \times M_r \times M_c$ antennas and all taps.

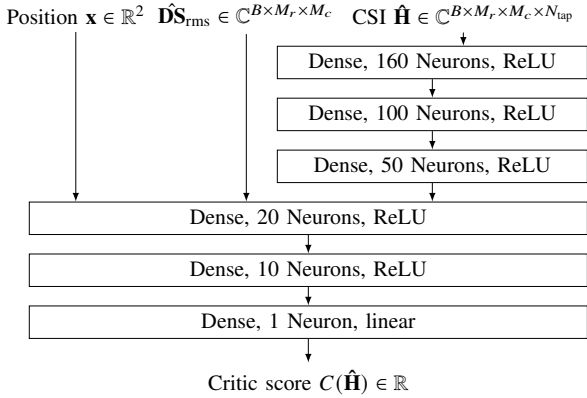
Generator and critic are dense neural networks, structured as shown in Fig. 4a and Fig. 4b. In the neural network, the complex-valued CSI is processed in separate real / imaginary parts, and conversion and reshaping layers are omitted from Fig. 4a and Fig. 4b for the sake of brevity. In addition to the raw generated CSI $\hat{\mathbf{H}}$, the critic is also provided antenna-specific root mean square (RMS) delay spread values derived from $\hat{\mathbf{H}}$, the computation of which is explained in Sec. V-A2. The behind providing RMS delay spread values is that they may aid the critic in scoring the realness of a generated sample. The WGAN is trained with GP [7] with GP coefficient $\lambda = 10$. Delay spread values and the conditional positions \mathbf{x} are normalized such that all numbers are in range $[-1, 1]$. The CSI, except for being split into real and imaginary parts, does not undergo any additional treatment like normalization.

IV. LINEAR INTERPOLATION BASELINE

To judge whether a GAN-based channel model is useful as an *interpolator*, we compare it to a simple classical interpolation baseline. While more advanced interpolation methods like,



(a) Structure of generator neural network G , with random noise input \mathbf{n} and condition \mathbf{x} (position)



(b) Structure of critic neural network C , where input $\hat{\mathbf{D}}\mathbf{S} \in \mathbb{C}^{B \times M_r \times M_c}$ denotes the normalized delay spread computed from $\hat{\mathbf{H}}$

Fig. 4. Structure of neural networks. Reshaping layers and the conversion from complex representation to separate real / imaginary parts are omitted.

for example, Kriging are well-known, we employ a simpler linear interpolation baseline: We construct the interpolant $F_{\text{interp}}: \mathbb{R}^2 \rightarrow \mathbb{C}^{B \times M_r \times M_c \times N_{\text{tap}}}$ by first computing the Delaunay triangulation of the two-dimensional training set positions, and then performing linear barycentric CSI interpolation on each triangle as follows: For a single triangle, let $\mathbf{s} \in \mathbb{R}^3$ denote the barycentric coordinate vector such that $\sum_i s_i = 1$ and let $\mathbf{H}^{(\Delta 1)}$, $\mathbf{H}^{(\Delta 2)}$, $\mathbf{H}^{(\Delta 3)}$ denote the CSI tensors of the corresponding vertices of the triangle. To account for unknown global starting phases $\varphi \in \mathbb{R}^3$ in the CSI tensors, we find the interpolated CSI tensor $\hat{\mathbf{H}}$ as the solution to the optimization problem

$$(\hat{\mathbf{H}}, \varphi) = \arg \min_{(\mathbf{H}, \varphi)} \sum_{i=1}^3 s_i \left\| \mathbf{H}^{(\Delta i)} - e^{j\varphi_i} \mathbf{H} \right\|_2^2,$$

where $\|\cdot\|_2$ is the straightforward generalization of the Euclidean norm to tensors and subtraction is applied elementwise. The optimization problem is solved by separate differentiation with respect to φ and \mathbf{H} , which yields a simple coordinate descent interpolation algorithm.

V. EVALUATION

Once GAN training has finished, the critic is no longer needed, and the generator can be evaluated. Depending on

whether one views the generative channel model as an *interpolator* or a *random generator*, one may want to consider different evaluation criteria. In this work, we compare both the spatial distributions of generated and measured CSI as well as stochastic CSI distributions. In contrast to generative models in image processing, where subjective human perception of the quality of a generated image can play an important role in the evaluation process, humans cannot easily interpret CSI data. Instead, we need to rely on human-interpretable quantities that can be derived from channel tensors $\hat{\mathbf{H}}$ to judge the generated data. For example, we can interpret and compare (to measured data) the distribution of powers, delay spreads or angular-domain properties in the generated data.

A. Evaluated Channel Parameters and Statistics

We focus our evaluation on three properties of the generated CSI, those being the received power, the delay spread and the angle of arrival (AoA). Furthermore, in an exemplary manner, we compare the delay spread distributions using the Jensen-Shannon distance (JSD).

1) *Received Power*: The total received power over all antennas in one antenna array b will be written as the norm

$$\|\mathbf{H}_b\|_{\text{F}}^2 = \sum_{m_r=1}^{M_r} \sum_{m_c=1}^{M_c} \sum_{t=1}^{N_{\text{tap}}} |\mathbf{H}_{b,m_r,m_c,t}|^2.$$

2) *Delay Spread*: For a single antenna in row m_r and column m_c of array b , the RMS delay spread is defined as

$$\text{DS}_{\text{rms},b,m_r,m_c} = \sqrt{\frac{\sum_t (t - \bar{t}_{b,m_r,m_c})^2 |\mathbf{H}_{b,m_r,m_c,t}|^2}{\sum_t |\mathbf{H}_{b,m_r,m_c,t}|^2}}$$

with $\bar{t}_{b,m_r,m_c} = \frac{\sum_t t |\mathbf{H}_{b,m_r,m_c,t}|^2}{\sum_t |\mathbf{H}_{b,m_r,m_c,t}|^2}$,

where $t = 1, \dots, N_{\text{tap}}$ is an index for the time tap. To interpret the results, we may also want to visualize the RMS delay spread averaged over all antennas in one array

$$\overline{\text{DS}}_{\text{rms},b} = \frac{1}{M_r M_c} \sum_{m_r=1}^{M_r} \sum_{m_c=1}^{M_c} \text{DS}_{\text{rms},b,m_r,m_c}.$$

By comparing the measured and generated RMS delay spread distribution, we can test if the GAN learns meaningful channel power delay profiles (PDPs).

3) *Angle of Arrival*: The array correlation matrix $\mathbf{R}^{(b)} \in \mathbb{C}^{M_c \times M_c}$ for the array with index b is estimated over all rows of the UPA. That is, $\mathbf{R}^{(b)}$ may be used to estimate the azimuth AoA, but contains no information about the elevation AoA:

$$\hat{\mathbf{R}}_{m_c1,m_c2}^{(b)} = \sum_{m_r=1}^{M_r} \sum_{t=1}^{N_{\text{tap}}} \mathbf{H}_{b,m_r,m_c1,t} \mathbf{H}_{b,m_r,m_c2,t}^* \in \mathbb{C}$$

Under the assumption of a single source, we apply the root-MUSIC algorithm to $\hat{\mathbf{A}}^{(b)}$ to find azimuth AoA estimates $\hat{\alpha}^{(b)}$ from $\hat{\mathbf{A}}^{(b)}$ for each datapoint and each UPA. An azimuth AoA of $\hat{\alpha}^{(b)} = 0^\circ$ indicates that the

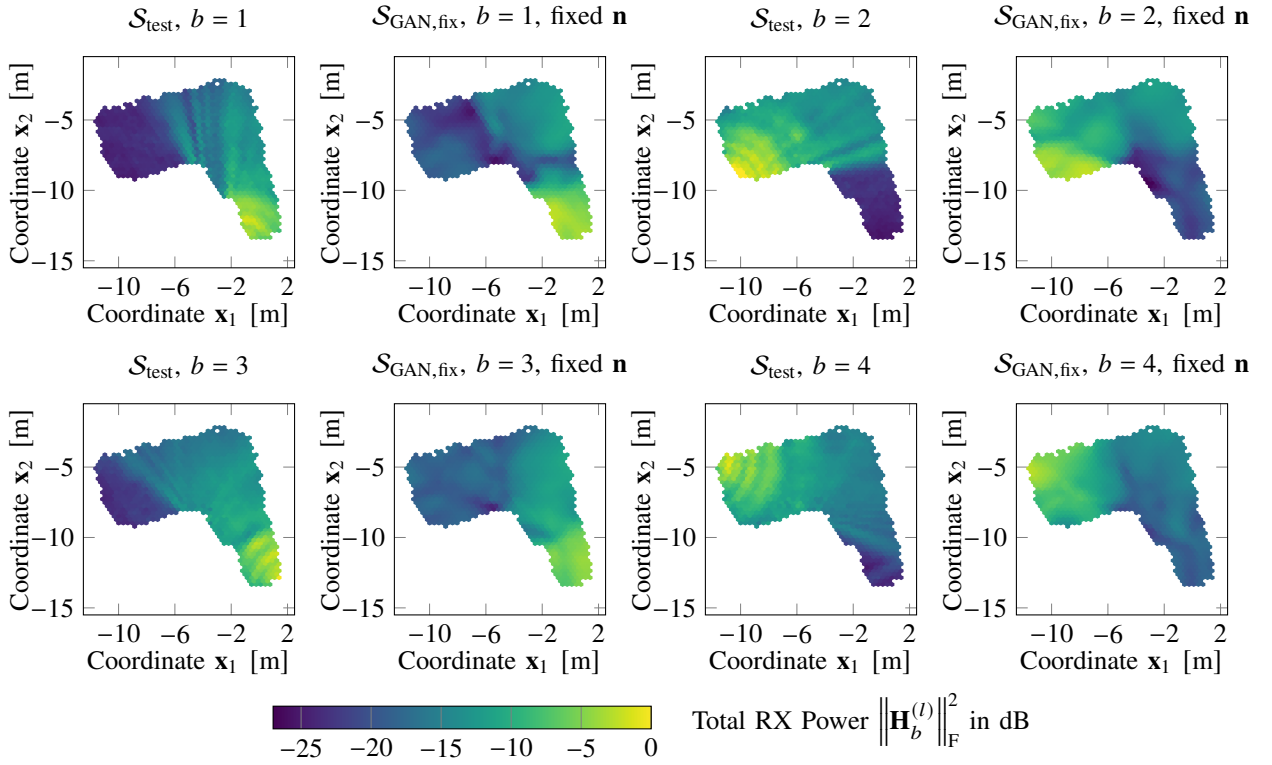


Fig. 5. Spatial distribution of received powers $\|\mathbf{H}_b^{(l)}\|_F^2$, for measured dataset $\mathcal{S}_{\text{meas}}$ and generated dataset $\mathcal{S}_{\text{GAN,fix}}$. The power is normalized such that the maximum received power (over *all* values $\|\mathbf{H}_b^{(l)}\|_F^2$, measured and generated) is 0 dB.

signal arrives directly from the front. By comparing measured and generated AoA distributions, we can test if the GAN learns a meaningful distribution of channel coefficient phases.

4) *Jensen-Shannon Distance*: Furthermore, to quantify the similarity of different stochastic distributions, we use the JSD. For two distributions P and Q over the same sample space \mathcal{X} , the JSD is defined as

$$d_{\text{JS}}(P||Q) = \sqrt{\frac{d_{\text{KL}}(P||M) + d_{\text{KL}}(Q||M)}{2}} \quad \text{with } M = \frac{P+Q}{2},$$

where d_{KL} is the Kullback-Leibler (KL) divergence, given by

$$d_{\text{KL}}(P||Q) = \sum_{x \in \mathcal{X}} P(x) \log \left(\frac{P(x)}{Q(x)} \right).$$

B. GAN Evaluation Procedure

To obtain a generated dataset \mathcal{S}_{gen} that is comparable to the test set $\mathcal{S}_{\text{test}}$, we use G to produce channel realizations for all positions $\mathbf{x}^{(l)}$ present in $\mathcal{S}_{\text{test}}$. Evaluating the generator can be approached in two ways:

- (I) The noise vector $\mathbf{n} \sim \mathcal{N}(0, 1)$ may be drawn once and then remain fixed over all positions (conditions) \mathbf{x} :

$$\mathcal{S}_{\text{GAN,fix}} = \left\{ \left(G \left(\mathbf{x}^{(l)}, \mathbf{n} \right), \mathbf{x}^{(l)} \right) \right\}_{(\mathbf{H}^{(l)}, \mathbf{x}^{(l)}) \in \mathcal{S}_{\text{test}}},$$

fixed $\mathbf{n} \sim \mathcal{N}(0, 1)$

- (II) The noise vector $\mathbf{n}^{(l)} \sim \mathcal{N}(0, 1)$ may be drawn randomly for each position (condition) $\mathbf{x}^{(l)}$:

$$\mathcal{S}_{\text{GAN,var}} = \left\{ \left(G \left(\mathbf{x}^{(l)}, \mathbf{n}^{(l)} \right), \mathbf{x}^{(l)} \right) \right\}_{(\mathbf{H}^{(l)}, \mathbf{x}^{(l)}) \in \mathcal{S}_{\text{test}}, \mathbf{n}^{(l)} \sim \mathcal{N}(0, 1)}$$

The first approach should lead to a higher level of spatial consistency in the generated CSI data, whereas the second approach can reveal what the generator has learned about the spatial channel distribution.

C. Linear Interpolator Evaluation Procedure

To generate CSI with the linear interpolation baseline, which makes use of the entire training set $\mathcal{S}_{\text{train}}$ to parametrize the interpolant, we evaluate the interpolant F_{interp} at the test set locations, yielding the interpolated CSI dataset:

$$\mathcal{S}_{\text{interp}} = \left\{ \left(F_{\text{interp}} \left(\mathbf{x}^{(l)} \right), \mathbf{x}^{(l)} \right) \right\}_{(\mathbf{H}^{(l)}, \mathbf{x}^{(l)}) \in \mathcal{S}_{\text{test}}}$$

D. Spatial Distribution Analysis

We consider the distribution of generated CSI relative to the two-dimensional spatial coordinates, which are passed to the GAN as condition. If the CSI generated by the GAN is similar to the test set CSI, this could indicate that GAN-based channel models are useful as *inter-/extrapolators*. First, we evaluate the generator output distribution according to approach (I), i.e., for fixed input noise \mathbf{n} . The corresponding received power distributions $\|\mathbf{H}_b^{(l)}\|_F^2$ for each antenna array $b = 1, \dots, 4$, both measured and generated for one particular noise realization, are shown in Fig. 5. Clearly, the WGAN has learned to produce CSI with some spatial consistency, and the spatial distribution of generated and measured channels is similar, but not identical. The generated channel realizations greatly depend on the choice of receiver antenna array b .

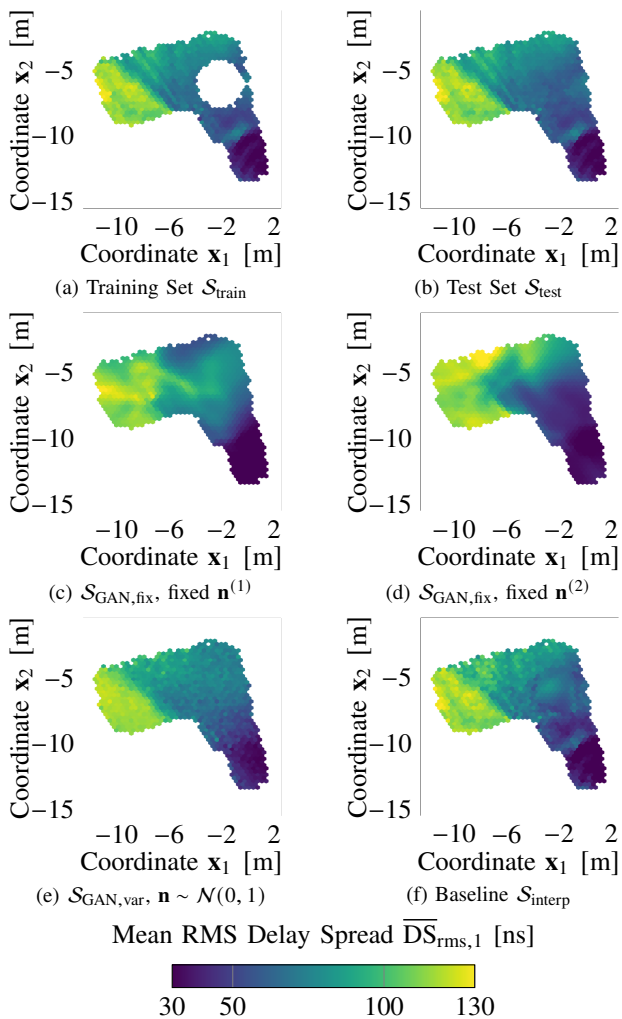


Fig. 6. RMS delay spread $\overline{DS}_{\text{rms},b}$, averaged over all antennas in array $b = 1$.

However, the neural network fails to produce CSI with true spatial consistency. For example, the concentric circles around the antenna arrays visible in the measured data (which are likely caused by a strong floor reflection) are not visible in the generated power distribution.

We can also analyze the RMS delay spread for approach (I). The results for array $b = 1$ are shown in Fig. 6c and Fig. 6d, for two different fixed noise vectors $\mathbf{n}^{(1)}$ and $\mathbf{n}^{(2)}$: It can be seen that the delay spread distributions depend on the noise vector and that they are also spatially consistent, yet distinct from the measured distribution. However, from Fig. 6f, it is also clear that the linear interpolation baseline produces CSI that much more closely resembles the test set if accurate CSI prediction is desired. Though not shown in Fig. 6, these observations also hold for antenna arrays $b = 2, 3, 4$. If we choose a random noise realization for every position \mathbf{x} as in approach (II), the spatial RMS delay spread distribution more closely resembles the test set, as visible in Fig. 6e.

The observed spatial distribution of received powers and delay spreads indicates that the generator was at least able to learn meaningful PDPs of the wireless channel. To test

d_{JS}	S_{train}	S_{test}	$S_{\text{GAN,var}}$	$S_{\text{GAN,fix}}$	S_{interp}	Gauss.
S_{train}	0.000	0.041	0.066	0.093	0.049	0.160
S_{test}	0.041	0.000	0.082	0.115	0.067	0.149
$S_{\text{GAN,var}}$	0.066	0.082	0.000	0.053	0.054	0.162
$S_{\text{GAN,fix}}$	0.093	0.115	0.053	0.000	0.070	0.191
S_{interp}	0.049	0.067	0.054	0.070	0.000	0.156
Gauss.	0.160	0.149	0.162	0.191	0.156	0.000

TABLE I

JSD BETWEEN VARIOUS RMS DELAY SPREAD DISTRIBUTIONS.

if the generator has also learned a meaningful distribution of phase information, we visualize the spatial distribution of AoA estimates generated by MUSIC for measured and generated CSI data in Fig. 7. Clearly, the GAN has captured the relationship between location and CSI phases to some extent, as indicated by the clearly visible gradient in the AoA estimates in Fig. 7c. The AoA estimate for the generated CSI corresponds to the true AoA of the LoS regions in the dataset. However, the linear interpolation baseline also clearly outperforms the GAN if the objective is to generate true-to-life CSI data: The AoA estimates for the interpolated CSI in Fig. 7d are almost identical to the AoA estimates generated for the test set in Fig. 7a. Fig. 7b, which shows the AoA estimate distribution for CSI generated by a GAN with fixed noise realization looks rather artificial: The individual AoA estimates for the generated CSI are all plausible for the specific position \mathbf{x} , but the spatial distribution is unrealistic, with constant AoA in some areas and rapid changes over space elsewhere. This may indicate that the generator has failed to produce CSI with meaningful spatial consistency.

Comparing test set distribution and generated distributions of received power, RMS delay spread and AoA estimates, we conclude that a GAN-based channel model is not a good spatial interpolator in our scenario, as even a simple linear interpolation baseline outperforms the GAN: Judging by RMS delay spread and AoA estimates, the interpolated CSI is clearly more similar to the test set than the GAN-generated CSI.

E. Stochastic Distribution Analysis

In the previous section, we compared the spatial distribution of generated CSI to the test set. If one is of the opinion that the GAN-based channel model should be used as a *random generator* for CSI that serves to generate CSI data with a certain stochastic distribution (and not to interpolate CSI), this is not a fair comparison. Therefore, we now compare the stochastic distribution of measured and generated CSI.

For the following analysis, we focus on the RMS delay spread only and disregard all spatial aspects. Of course, these analyses could also be performed on other CSI properties like received power or angular-domain information, with similar conclusions. We estimate the density function of the RMS delay spreads over all antennas in all antenna arrays for measured and generated CSI by binning delay spreads into 150 bins. In addition, we compare the generated RMS delay spread distribution to randomly drawing from a Gaussian probability density function (PDF), whose first- and second-order moments are directly estimated from the training set's RMS delay spread distribution.

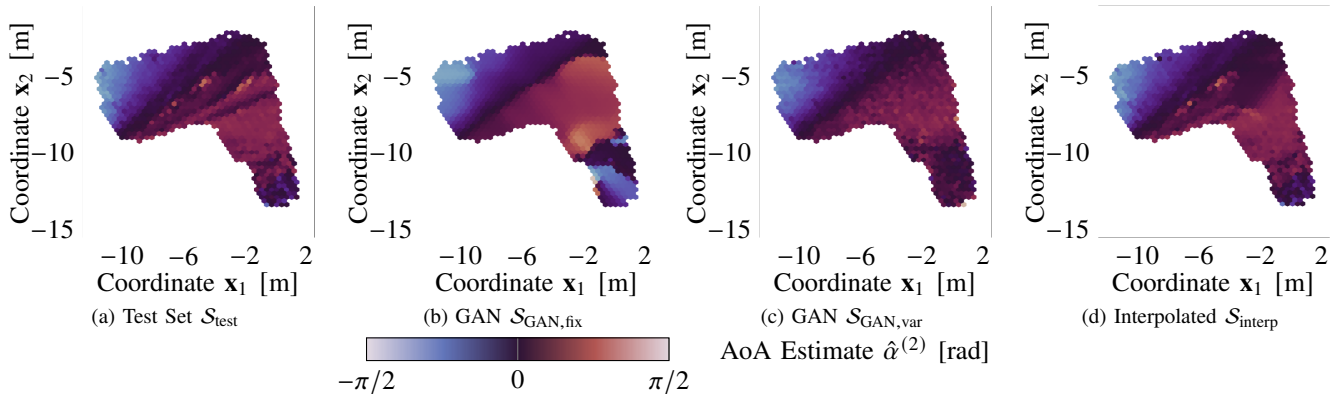


Fig. 7. Spatial azimuth AoA estimate distribution for antenna array $b = 2$ for various measured / generated CSI datasets. Note that the color map is circular.

The resulting histograms and the parametrized Gaussian distribution are shown in Fig. 8. The high degree of similarity between the measured and generated histograms indicates that the GAN is able to approximate the measured channel distribution well, but so is the linear interpolator. Furthermore, the histogram indicates that the GAN not only learned the first and second-order moments of the delay spread distribution, but also higher-order moments. If one were instead to sample RMS delay spreads for a generative stochastic model from an estimated Gaussian distribution, the resulting CSI distribution would be a bad approximation of the realistic CSI. Please note that the RMS delay spread distribution for $\mathcal{S}_{\text{GAN,fix}}$ depends on the particular random noise input \mathbf{n} , so the density shown here is only exemplary.

To quantify the similarity of the densities in Fig. 8 more objectively, we compute the JSDs between any two density functions, resulting in the JSD distance matrix shown in Tab. I. Unsurprisingly, the RMS delay spread distribution that most closely resembles the test set is the training set, followed by the interpolated CSI. The RMS delay spread distribution generated by the GAN is less similar than the interpolated CSI, but still much better than sampling from a Gaussian distribution.

We conclude that in our scenario, the GAN-based channel model was able to reproduce the statistical CSI distribution, at least when judged on the basis of the delay spread of generated CSI. However, the CSI that the GAN generates is highly specific to the considered setup and environment.

VI. CRITICISM

Neural networks show promising results for various communications-related applications, including channel coding [18], channel charting [19], and channel prediction [20]. What these applications have in common is that there is a lot of training data available, but there is no good system model due to the unknown statistical properties of the propagation channel. Clearly, under these circumstances, machine learning can lead to significant improvements. On the face of it, the same logic applies to GAN-based channel modeling, where large CSI datasets are available for training. However, upon closer inspection, this impression is deceptive: Just because there is a lot of training data available does not necessarily mean that the training data is suitable for training a useful

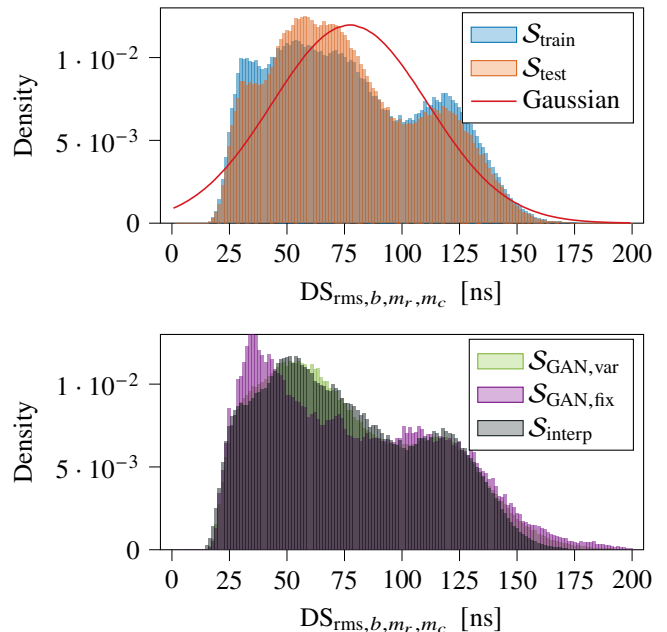


Fig. 8. Density functions of RMS delay spread distributions for various CSI datasets and Gaussian approximation.

generative model. In the following, we outline why we believe GAN-based channel modeling (and generative neural network-based channel modeling in general) is not ready for practical use in its current form. In Sec. V-D we already concluded that GAN-based channel models are not good interpolators. Here, we argue that in their current form, they are also not good GSCM replacements and that significant architectural changes are necessary for them to become useful.

A. Lack of generalizability

A GAN-based channel model is trained on one particular dataset or a collection of CSI datasets captured with the same setup. The current system architecture would not allow for training the same generator on datasets captured in different environments with different antenna setups. Therefore, the GAN-based channel model is always specific to the environment it was trained for and, in contrast to a GSCM, cannot generalize to a different number of antennas, antenna deployments, carrier frequencies or other environment parameters.

B. Lack of meaningful spatial consistency

Spatial consistency is an important concept in channel modeling: In GSCMs, it can be ensured in various ways, e.g., by defining scattering clusters [3], or by modeling spatial correlations of stochastic distributions like, for example, spatially correlated shadow fading [21]. Judging by the results in Sec. V-D, it may seem like the GAN ensures at least some level of spatial consistency. This is the case in the sense that the GAN generates a CSI sample that is plausible for the considered position (condition) \mathbf{x} . However, it does not mean that the GAN ensures any meaningful spatial correlation between two generated CSI samples $\hat{\mathbf{H}}^{(1)}$ and $\hat{\mathbf{H}}^{(2)}$ at different locations $\mathbf{x}^{(1)}$ and $\mathbf{x}^{(2)}$. In fact, we found that the level of spatial correlation depends on the range to which the condition \mathbf{x} is normalized. This indicates that spatial correlation is not inferred from the training data, but is merely an artifact of the network architecture and training procedure.

C. Lack of interpretability

One of the strengths of channel models is the ability to see how a designed system would perform under different conditions. For example, a system designer may want to understand how the system performs at different carrier frequencies, for different antenna deployments, Doppler spreads, path loss exponents or noise distributions. Other than in GSCMs, these properties are not controlled in GAN-based channel models. If a developed system or algorithm shows good or poor performance on a specific GAN-based channel model, it would be difficult to understand why that is the case.

D. Availability of a dataset

The results in Sec. V-E indicate that using a GAN-based channel model is only applicable if the objective is to have a channel model for the particular environment that the measured (or simulated) training dataset was captured in. In that case, a GAN can generate CSI that follows the distribution of the training dataset. However, if the objective is to produce CSI that is as similar as possible to a training set, one may just as well use the training dataset itself. If the dataset is too small, one could use various classical data augmentation techniques (e.g., adding noise, adding random global phase rotations) or interpolation, rendering the generative model unnecessary.

VII. CONCLUSION

We have demonstrated that a GAN can be used to learn the statistical distribution of CSI in a measured dataset. GANs can capture higher-order channel statistics, without requiring manual extraction of parameters, and, by conditioning, can generate plausible CSI for arbitrary positions. However, as presented here, GAN-based channel modeling still has many downsides compared to GSCMs, some important ones being the inferior interpretability, lack of meaningful spatial consistency and limited flexibility of the model: The channel model is only valid for the particular environment and antenna deployment of the dataset. For these reasons, we have come to the conclusion that GAN-based channel models are not

good interpolators and are also not useful as general-purpose GSCMs in their current form. Achieving that would likely require more, and more diverse training data and a different architectural approach. For example we could imagine using GANs in conjunction with raytracing-based channel models, where a generative model creates a radio environment, and the raytracer computes spatially consistent CSI.

REFERENCES

- [1] R. H. Clarke, "A statistical theory of mobile-radio reception," *Bell system technical journal*, vol. 47, no. 6, pp. 957–1000, 1968.
- [2] ETSI 3rd Generation Partnership Project (3GPP), "Study on channel model for frequencies from 0.5 to 100 GHz (3GPP TR 38.901 version 16.1.0 Release 16)," ETSI, Tech. Rep., 2020.
- [3] F. Burkhardt, S. Jaeckel, E. Eberlein, and R. Prieto-Cerdeira, "QuaDRiGa: a MIMO Channel Model for Land Mobile Satellite," in *The 8th European Conference on Antennas and Propagation (EuCAP 2014)*. IEEE, 2014, pp. 1274–1278.
- [4] J. Hoydis *et al.*, "Sionna RT: Differentiable Ray Tracing for Radio Propagation Modeling," *arXiv preprint*, Mar. 2023.
- [5] I. Goodfellow *et al.*, "Generative Adversarial Nets," *Advances in neural information processing systems*, vol. 27, 2014.
- [6] M. Arjovsky, S. Chintala, and L. Bottou, "Wasserstein Generative Adversarial Networks," in *International conference on machine learning*. PMLR, 2017, pp. 214–223.
- [7] I. Gulrajani, F. Ahmed, M. Arjovsky, V. Dumoulin, and A. C. Courville, "Improved Training of Wasserstein GANs," *Advances in neural information processing systems*, vol. 30, 2017.
- [8] Y. Yang, Y. Li, W. Zhang, F. Qin, P. Zhu, and C.-X. Wang, "Generative-Adversarial-Network-Based Wireless Channel Modeling: Challenges and Opportunities," *IEEE Communications Magazine*, vol. 57, 2019.
- [9] H. Xiao, W. Tian, W. Liu, and J. Shen, "ChannelGAN: Deep learning-based channel modeling and generating," *IEEE Wireless Communications Letters*, vol. 11, no. 3, pp. 650–654, 2022.
- [10] T. Orekondy, A. Behboodi, and J. B. Soriaga, "MIMO-GAN: Generative MIMO Channel Modeling," in *JCC 2022-IEEE International Conference on Communications*, 2022, pp. 5322–5328.
- [11] W. Xie, M. Xiong, Z. Yang, W. Liu, L. Fan, and J. Zou, "Real and fake channel: GAN-based wireless channel modeling and generating," *Physical Communication*, p. 102214, 2023.
- [12] U. Sengupta, C. Jao, A. Bernacchia, S. Vakili, and D. Shiu, "Generative Diffusion Models for Radio Wireless Channel Modelling and Sampling," *arXiv preprint arXiv:2308.05583*, 2023.
- [13] J. Juhava, "Wireless channel modeling using generative machine learning models," Master's thesis, Aalto University School of Engineering, 2023.
- [14] T. J. O'Shea, T. Roy, and N. West, "Approximating the Void: Learning Stochastic Channel Models from Observation with Variational Generative Adversarial Networks," in *2019 International Conference on Computing, Networking and Communications (ICNC)*. IEEE, 2019.
- [15] S. Dörner, M. Henninger, S. Cammerer, and S. ten Brink, "WGAN-based Autoencoder Training Over-the-air," in *2020 IEEE 21st International Workshop on Signal Processing Advances in Wireless Communications (SPAWC)*. IEEE, 2020, pp. 1–5.
- [16] F. Euchner, M. Gauger, S. Dörner, and S. ten Brink, "A Distributed Massive MIMO Channel Sounder for "Big CSI Data"-driven Machine Learning," in *25th Workshop on Smart Antennas*, 2021.
- [17] F. Euchner and M. Gauger, "CSI Dataset dichasus-cf0x: Distributed Antenna Setup in Industrial Environment, Day 1," 2022. [Online]. Available: <https://doi.org/doi:10.18419/darus-2854>
- [18] T. Gruber, S. Cammerer, J. Hoydis, and S. ten Brink, "On Deep Learning-Based Channel Decoding," in *2017 51st annual conference on information sciences and systems (CISS)*, 2017, pp. 1–6.
- [19] C. Studer, S. Medjkouh, E. Goultas, T. Goldstein, and O. Tirkkonen, "Channel Charting: Locating Users Within the Radio Environment Using Channel State Information," *IEEE Access*, vol. 6, 2018.
- [20] W. Jiang and H. D. Schotten, "Neural Network-Based Fading Channel Prediction: A Comprehensive Overview," *IEEE Access*, vol. 7, 2019.
- [21] X. Cai and G. B. Giannakis, "A Two-Dimensional Channel Simulation Model for Shadowing Processes," *IEEE Transactions on Vehicular Technology*, vol. 52, no. 6, pp. 1558–1567, 2003.